Enhancement of Turbulence in Tokamaks by Magnetic Fluctuations

B. N. Rogers and J. F. Drake
Institute for Plasma Research, University of Maryland, College Park, Maryland 20742
(Received 11 February 1997)

Three-dimensional nonlinear simulations of drift-ballooning modes in a torus including electromagnetic effects are described. When diamagnetic effects are weak, the self-consistent magnetic fluctuations in the model lead to a drastic enhancement of the transport well below the ideal ballooning instability limit. [S0031-9007(97)03596-5]

PACS numbers: 52.30.Jb, 52.25.Fi, 52.35.Ra, 52.55.Fa

The ability to predict fluctuation driven heat and particle transport in tokamaks is vital to the accurate design of future fusion machines of practical interest. As a result, intense effort (see, e.g., Refs. [1–9]) has been focused on the development of realistic numerical models of the turbulent processes leading to this transport. These models are conventionally based on the electrostatic approximation, in which the fluctuations of the magnetic field generated by the plasma turbulence are neglected. We show here that in the edge region of tokamaks these fluctuations are essential to the description of high-performance discharges, and can lead to drastic enhancements in the predicted transport rates unless diamagnetic effects are sufficiently strong. This enhancement is caused by the influence of magnetic field line bending and shear on self-generated radial plasma flows in the system. In an electromagnetic model, such motions create radial magnetic field perturbations, which effectively stiffen the flow and inhibit its tendency to break up and become turbulent. As a result, stronger flows, and thus stronger transport, are sustained.

The simulations are carried out in a poloidally and radially localized, flux-tube-like domain that winds around the torus [7]. Assuming a shifted-circle magnetic geometry, the equations for perturbations of the density n, potential ϕ, magnetic flux ψ, and parallel flow $v_\parallel$ are as follows:

$$d_t n + \partial_y \phi - \epsilon_n C(\phi - \alpha_d n) + (1+\tau)\alpha_d \epsilon_n \nabla_\parallel J + \epsilon_v \nabla_\parallel v_\parallel = 0, \quad (1)$$

$$\nabla_\perp \cdot d_t \nabla_\perp (\phi + \tau \alpha_d n) + Cn + \nabla_\parallel J = 0, \quad (2)$$

$$(2\pi)^2 \alpha(\partial_t \psi + \alpha_d \partial_y \psi) + \nabla_\parallel(\phi - \alpha_d n) = J, \quad (3)$$

$$d_t v_\parallel + \epsilon_v[\nabla_\parallel n - (2\pi)^2 \alpha \partial_y \psi] = 0, \quad (4)$$

where $J = \nabla_\perp^2 \psi$, $C = [\cos(2\pi z) + h(z)\sin(2\pi z) - \epsilon]\partial_y + \sin(2\pi z)\partial_x$ is the curvature operator, $h(z) = 2\pi \hat{s} z - \alpha \sin(2\pi z)$, $d_t = \partial_t + \hat{z} \times \nabla\phi \cdot \nabla$, $\nabla_\parallel = \partial_z - (2\pi)^2 \alpha \hat{z} \times \nabla\psi \cdot \nabla$, $\nabla_\perp^2 = [\partial_x + h(z)\partial_y]^2 + \partial_y^2$. For simplicity, T_i and T_e are assumed to be constant in the simulations described here. However, further simulations including the contribution of the η_i mode (for example) have been carried out, and the main results we discuss exhibit no qualitative change. The coordinate z lies along the equilibrium magnetic field $\vec{B}_0$, and the ambient density gradient is in the x direction. The parallel, perpendicular, and time normalization scales are, respectively, $L_z = 2\pi qR$, $L_0 = 2\pi q(\nu_{ei} R\rho_s/2\Omega_e)^{1/2}(2R/L_n)^{1/4}$, and $t_0 = (RL_n/2)^{1/2}/c_s$ (the ideal ballooning time), where $c_s^2 = T_e(1+\tau)/m_i$, $\rho_s = c_s/\omega_{ci}$, and $\tau = T_i/T_e$. Other parameters are the magnetic shear $\hat{s} = r(dq/dr)/q$, the magnetohydrodynamic (MHD) ballooning parameter $\alpha = -Rq^2 d\beta/dr$, the diamagnetic parameter $\alpha_d = \rho_s c_s t_0/L_n L_0$, $\epsilon = r/R$, $\epsilon_n = 2L_n/R$, $\epsilon_v = c_s t_0/L_z$, with L_n the equilibrium density (or pressure) scale length. Unless otherwise noted, we consider the typical values $\hat{s} = 1$, $\tau = 1$, $\epsilon = 0.2$, $\epsilon_n = 0.05$, $\epsilon_v = 0.02$. In these units $n/n_0 \sim v_z/c_s \sim L_0/L_n$, $\phi \sim BL_0^2/ct_0$, and $\psi \sim 2\pi\alpha B_0 L_0^2/qR$. Realistic diffusive dissipation terms are added to each equation.

Aside from the α term in $h(z)$ that arises from the Shafranov shift of the flux surfaces, the terms proportional to α in Eqs. (1)–(4) represent the contribution of the magnetic field perturbations. These terms underlie the ideal MHD ballooning instability threshold, which occurs for $\alpha \sim 1$. For $\alpha \ll 1$ the magnetic terms can be neglected, and the system becomes effectively electrostatic. A main finding of this study is the magnetic fluctuations can have a large impact on the nonlinear behavior even at modest values of $\alpha \sim 0.1 - 0.2$.

The strong α dependence of the simulations arises from an inherently nonlinear effect, and is not consistent with expectations based on linear theory. To demonstrate this, we describe the results of a linear ballooning mode stability analysis of Eqs. (1)–(4). We address first a case in which diamagnetic effects are weak with $\alpha_d = 0.1$. The solid curves shown in Fig. 1(a) are the growth rates versus α for two values of the poloidal wave number: $k_\theta = 7$ (upper curve) and $k_\theta = 1$ (lower curve). The dashed curves in Fig. 1(a) show the electrostatic results. Finally, the dotted curve shows the ideal growth rate, with $\alpha_d \longrightarrow 0$. This curve defines the first ($\alpha < 0.8$) and second ($\alpha > 2.1$) stability regions obtained in the ideal limit of our model. A comparison of the solid and dashed curves shows that electromagnetic effects, while

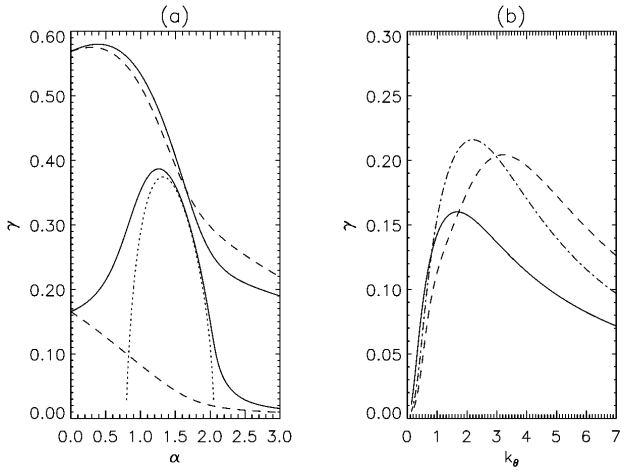

FIG. 1. (a) γ vs α at $\alpha_d = 0.1$; (b) γ vs k_θ at $\alpha_d = 0.5$.

having little impact on shorter wavelengths $\lambda \sim 1$, can be strongly destabilizing at longer wavelengths for $\alpha \sim 1$.

The growth rates at higher values of the diamagnetic parameter and their dependence on α are substantially reduced. Figure 1(b) shows γ versus k_θ at $\alpha_d = 0.5$, for two different values of α: 0 (dot-dashed curve) and 0.7 (solid curve—electromagnetic; dashed curve—electrostatic). These curves show that γ in the electromagnetic model (below the ideal threshold) is a mostly decreasing function of α, and exhibits only a modest enhancement at small k_θ relative to the electrostatic limit even for $\alpha = 0.7$.

We now turn to nonlinear simulations of Eqs. (1)–(4), which show an α dependence stronger than that just described. These simulations are started from small amplitude random perturbations, which develop into a coherent pattern of radial streams consistent with the structure of a dominant, linearly unstable mode. As in the example shown in Fig. 2, at some point [$t \simeq 23$ in Fig. 2(a)] these streams break up due to the onset of a secondary instability [see Fig. 2(b)], which quickly leads to saturation and fully developed turbulence. We focus on the α dependence of the radial particle flux Γ in this turbulent state, averaged over time and poloidal angle. An expression for this quantity may be obtained by integrating Eq. (1) over y and z, and in the general case contains some terms proportional to $\partial_y \psi$ (i.e., B_x). These magnetic terms, however, are found to make a negligible contribution to Γ in the nonlinear simulations that follow (much smaller than would be expected on the basis of test-particle estimates, for example), so $\Gamma \simeq \langle n V_x \rangle$ with $V_x = -\partial_y \phi$.

The results for Γ are shown in Fig. 3. The solid curves represent electromagnetic simulations, while the dashed curves show the electrostatic results. The two sets of curves are for $\alpha_d = 0.1$ (squares) and $\alpha_d = 0.5$ (triangles). For $\alpha_d = 0.1$, the electromagnetic and electrostatic models produce comparable fluxes for $\alpha < 0.1$. As α is raised, however, the particle (and energy) fluxes in the electromagnetic model increase dramatically. At $\alpha = 0.3$, still less than 50% of the ideal mode threshold, these fluxes have increased by about a factor of 6 above the electrostatic values.

As seen from the $\alpha_d = 0.5$ results in Fig. 3 (triangles), the flux levels in the electromagnetic model are very sensitive to diamagnetic effects. At $\alpha = 0.3$, the large enhancement in Γ found for $\alpha_d = 0.1$ is eliminated (although a residual 40% enhancement of $\langle n^2 \rangle$ is still observed). Simulations at other values of T_i/T_e (not shown) indicate this reduction is due mainly to ω_{*e} rather than ω_{*i}. (We find ω_{*i} effects become increasingly important at still higher levels of α_d and α—this will be addressed in a future article.) At the larger value of $\alpha = 0.5$ in Fig. 3, a fourfold enhancement in Γ returns. The electromagnetic simulations at both small and large α_d also display a shift in the dominant modes to longer wavelengths relative to the electrostatic case. This is visible in Fig. 4, which shows the density perturbations in the electromagnetic [Fig. 4(a)] and electrostatic [Fig. 4(b)] models for $\alpha = 0.3$, $\alpha_d = 0.1$.

We now address the mechanisms underlying this behavior. It might seem the enhancement of transport could be a reflection of the destabilizing influence of the ideal mode in the linear system. This is not the case. One indication of this is the early onset of the enhancement,

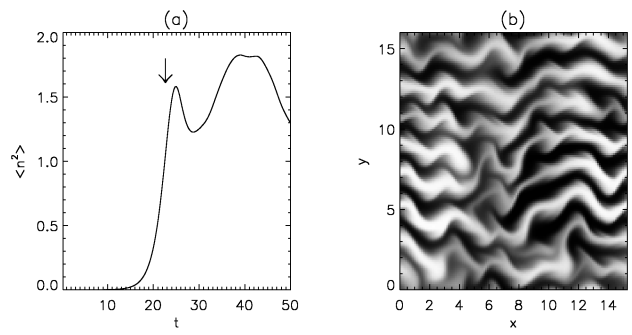

FIG. 2. (a) Typical evolution of $\langle n^2 \rangle$; (b) density perturbations at $t \simeq 23$.

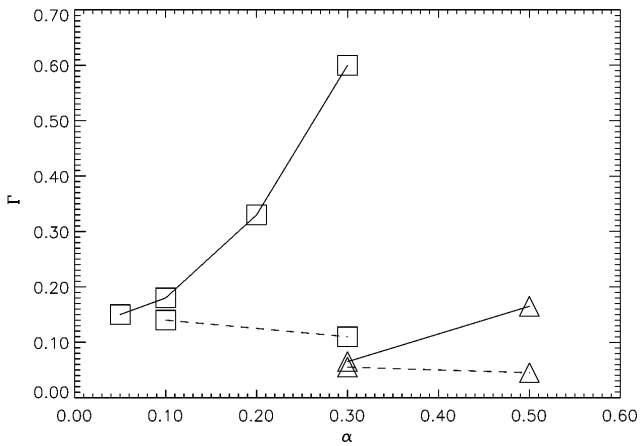

FIG. 3. Normalized particle flux Γ vs α.

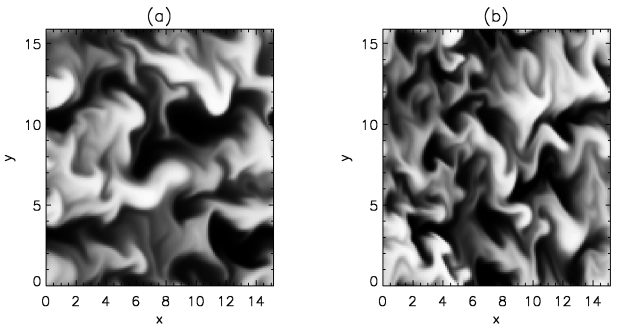

FIG. 4. Density perturbations: (a) electromagnetic, (b) electrostatic.

which can become large for values of $\alpha \sim 0.2$ at which the change in the linear mode for any k_θ is small. The real proof, however, is that the enhancement can be virtually eliminated by excluding the purely nonlinear contribution of the magnetic perturbations to $\nabla_\parallel$ in the vorticity equation (2) and Ohm's law (3). Since saturation of the system is initially caused by secondary instabilities like those in Fig. 2, these magnetic terms for small α_d must delay the onset of such instabilities and thereby allow the fundamental modes to reach larger amplitudes before the break-up process is triggered. Conversely, at larger α_d, the relative insensitivity of the saturation amplitudes to α indicates the secondary modes relevant to this case have a different character, and depend more weakly on the magnetic perturbations.

To gain some qualitative insight into this behavior, we apply Eqs. (1)–(4) to the stability analysis of a one-dimensional model, similar to the radially streaming configuration of Fig. 2, i.e., an unstable ballooning mode with characteristic wave number k_b and growth rate γ_b. We take $\phi \sim \psi \sim n \sim \exp(ik_b y)$, with amplitude coefficients ϕ_b, ψ_b, etc. obtained from a numerical solution of the linear ballooning mode equation. We eliminate the z dependence of the linear solution by an effective average along z. Thus, the model configuration depends on y only, and we consider the behavior of linear perturbations that vary as $f(y)\exp(\gamma t + ik_x x + ik_z z)$.

Linearizing Eqs. (1)–(4) about an arbitrary, real y-dependent configuration, we find

$$\gamma_v(\tilde{\phi}'' - k_x^2\tilde{\phi}) - \gamma_v''\tilde{\phi} = -ik_\parallel(\tilde{\psi}'' - k_x^2\tilde{\psi}) + ik_\parallel''\tilde{\psi} - C\tilde{n}, \quad (5)$$

$$\tilde{\psi}'' - k_x^2\tilde{\psi} = ik_\parallel(\tilde{\phi} - \alpha_d\tilde{n}) + \hat{\alpha}\gamma_v\tilde{\psi}, \qquad \gamma_v\tilde{n} = -ik_x n'\tilde{\phi}, \quad (6)$$

where primes denote d/dy, $\hat{\alpha} \equiv (2\pi)^2\alpha$, $\gamma_v = \gamma + ik_x V_x$, $k_\parallel = k_z + k_x B_x$, $V_x = -\phi'$, $B_x = \hat{\alpha}\psi'$. For simplicity, we exclude terms arising from the ambient density gradient and take $\epsilon_v = \epsilon_n = \tau = 0$. We have analyzed Eqs. (5) and (6) numerically for the configuration described above with periodic boundary conditions. At small α_d, this analysis shows the strongest secondary modes are driven by the velocity shear [γ_v'' in Eq. (5)], the magnetic curvature [$C\tilde{n}$ in (5)], and magnetic reconnection [$k_\parallel''$ in (5)]. As expected from the simulations, the system in this regime is controlled by the stabilizing effect of the magnetic field mentioned earlier, and displays an instability criterion with a strong dependence on the magnetic terms in $k_\parallel$. In contrast, at larger $\alpha_d \sim 1$ the strongest mode is a drift wave instability [driven by the n' term in Eq. (6)]. This mode has a different dependence on $k_\parallel$ than those at small α_d, and is influenced in a weaker, more complex way by the background magnetic perturbation. Consistent with the simulations, the strong enhancement in the transport found at small α_d is therefore not expected in this case.

We first analyze the case in which only the velocity gradient instability is present, and then consider the addition of the electromagnetic terms. For simplicity, we exclude the contribution of the magnetic curvature in this analysis, although our results indicate it is in general competitive with the velocity shear effects, and depends on magnetic line bending in a similar way. Finally, we address the regime of larger α_d.

When the curvature, electromagnetic, and diamagnetic terms are absent, only the Kelvin-Helmholz instability remains. This mode has a maximum growth rate $\gamma_{\max} \simeq 0.3k_b^2|\phi_b|$ at $k_x \simeq 0.6k_b$ and $k_z = 0$. Since the present quasistatic treatment becomes relevant for $\gamma_{\max} > \gamma_b$, we estimate the onset amplitude of instability with the condition $\gamma_{\max} \sim \gamma_b$, which gives $|\phi_b| \simeq 3.7\gamma_b/k_b^2$. (For the secondary mode to be effective, one might also require $k_\perp \sim k_b$—a condition which is satisfied for the cases discussed here.) Denoting $V_b = k_b|\phi_b|$, this $\alpha = 0$ result is the solid curve in Fig. 5. The drop in V_b seen at small k_b is due to the decline of γ_b at long wavelength.

At finite α values, the magnetic perturbation ψ_b associated with the ballooning mode enters through its contribution to $k_\parallel$, and has a very stabilizing impact on the Kelvin-Helmholz mode. Its importance can be

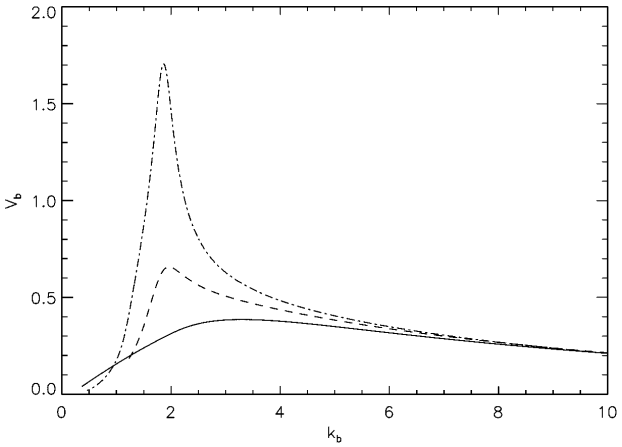

FIG. 5. Onset amplitude $V_b(k_b)$ of secondary modes.

estimated by retaining the simplest addition from line bending: Dropping the $k_\parallel''$ term in Eq. (5) and the $\alpha\gamma_v\psi$ term in Eq. (6), the right hand side of Eq. (5) reduces to $k_\parallel^2\hat{\phi}$. This line bending term becomes comparable to the terms on the left hand side of Eq. (5) for $k_\parallel^2/k_\perp^2 \gtrsim \gamma$, or with $\gamma \sim \gamma_b$, $k_\perp \sim k_b$, and $k_\parallel \sim \hat{k}_x B_x \sim \hat{\alpha} k_b^2 \psi_b$, for $\hat{\alpha}^2 k_b^2 \psi_b^2 \gtrsim \gamma_b$. An expression for ψ_b can be obtained from Ohm's law, $J \sim k_b^2\psi_b \sim \nabla_\parallel\phi \sim \phi_b$, and the Kelvin-Helmholtz onset criterion, $\phi_b \sim \gamma/k_b^2 \sim \gamma_b/k_b^2$, which give $\psi_b \sim \gamma_b/k_b^4$. Thus, line bending becomes important for $k_b \lesssim \gamma_b^{1/6}\hat{\alpha}^{1/3}$. This expression demonstrates that the Kelvin Helmholz stability of long wavelength radial streams is sensitive to electromagnetic effects even at very small values of α. For example, estimating $k_b \sim 1-2$ (see Fig. 4), this condition yields $\alpha\ [= \hat{\alpha}/(2\pi)^2] \gtrsim 0.1$–$0.3$, which is roughly consistent with the onset of enhanced transport in Fig. 3.

This scaling argument suggests the possibility of a long-wavelength catastrophe, in which modes at sufficiently long wavelength, stabilized by the magnetic perturbations, grow without bound. This trend is seen in Fig. 5, which shows the onset amplitude of instability of the radial streams including all the electromagnetic terms for $\alpha = 0.3$ (dashed line) and $\alpha = 0.5$ (dot-dashed line). For finite α the onset amplitude increases sharply with decreasing k_b down to $k_b \sim 2$, consistent with our scaling analysis. Below $k_b \sim 2$, however, the emergence of a new, electromagnetic instability leads to a sudden drop in the two curves with finite α. The B_x perturbations, produced by the periodic streams, alternate in sign as a function of y, and at long wavelength are broken up by a periodic double tearing mode. The maximum double tearing growth rate [10], obtained for $k_x \sim k_b$, is given by $\gamma \sim |k_b^3\psi_b|^{2/3}$, or with the expression $\psi_b \sim \phi_b/k_b^2 \equiv V_b/k_b^3$ presented earlier, $\gamma \sim V_b^{2/3}$. The onset condition $\gamma \sim \gamma_b$ is therefore satisfied for $V_b \sim \gamma_b^{3/2}$, which decreases rapidly for $k_b \longrightarrow 0$, consistent with Fig. 5. For increasing k_b, the mode is progressively stabilized by velocity shear. This stabilization becomes important when $k_x V_x(x \sim \Delta) \gtrsim \gamma$, where $\Delta \sim 1/(\hat{\alpha}\gamma)^{1/2}$ is the scale length of the reconnection region [10]. Given $k_x \sim k_b$ and $\gamma \sim V_b^{2/3}$, this can be written as $k_b \gtrsim \hat{\alpha}^{1/4}$, yielding $k_b \gtrsim 2$ for $\alpha \sim 0.3$–0.6. The stabilization of the tearing mode by velocity shear for increasing k_b ($k_b \gtrsim \hat{\alpha}^{1/4}$), and stabilization of the Kelvin Helmholz instability for decreasing k_b ($k_b \lesssim \gamma_b^{1/6}\hat{\alpha}^{1/3}$), leads at finite $\alpha \gtrsim 0.3$ to a wave number "gap," centered on $k_b \simeq 2$, in which no strong secondary modes exist. The peak in Fig. 5 at $k_b \simeq 2$ reflects this gap, and indicates that ballooning modes in this part of the spectrum can reach substantially enhanced amplitudes in the electromagnetic model before the onset of secondary modes.

Finally, we address the case of larger $\alpha_d \sim 0.5$. The simulations exhibit a weaker dependence on α in this case, and this is consistent with the results we obtain from Eqs. (5) and (6). We consider a simplified limit $\gamma_v \longrightarrow \gamma$, $n' = \text{const}$, $k_\parallel = \text{const}$, $C \longrightarrow 0$, and retain the magnetic terms only in $k_\parallel$. One then obtains a complex growth rate associated with a drift-wave instability $\gamma = -\mu^2 + (\mu^4 - 2i\mu^2\Omega_{*e})^{1/2}$, with $\Omega_{*e} = -\alpha_d k_x n'$ and $\mu^2 = k_\parallel^2/2k_\perp^2$. In contrast to the velocity gradient (or curvature) driven modes discussed earlier, which are most unstable for $k_\parallel \longrightarrow 0$, this mode *requires* a finite value of $k_\parallel$ to be unstable. The most unstable value, found by maximizing $\gamma_r = \mathrm{Re}(\gamma)$ over $k_\parallel$, is $k_\parallel^2 \simeq k_\perp^2|\Omega_{*e}|$, and gives $\gamma_{r,\max} \simeq 0.3|\Omega_{*e}|$. Thus, the contribution of $k_\parallel$ is no longer uniformly stabilizing, and the magnetic suppression of secondary instability found earlier is no longer observed.

Based on experience from linear theory alone, one would not expect either the drift wave or electromagnetic effects to play a major qualitative role in the regimes considered here. As is well known, the drift wave is linearly stable in a system with magnetic shear. Nonlinearly, however, we find both effects are essential due to their vital impact on the saturation process. These results, although not directly applicable to the hotter tokamak core region, imply that it may be appropriate to reevaluate the role of such effects in models of core transport, in which the electrons are assumed to be adiabatic and thus drift-wave dynamics and magnetic perturbations are neglected.

In conclusion, the transport predicted by the electromagnetic model depends strongly on the level of diamagnetic effects. When diamagnetic effects are sufficiently weak, self-generated magnetic fluctuations in our simulations lead to a β-dependent enhancement of the transport levels. This enhancement becomes very large as the system approaches a small fraction ($\sim 1/4$) of the ideal MHD stability limit. These results, though they do not address some important effects associated with realistic experimental profiles, indicate an electromagnetic model is essential to the reliable modeling of edge region transport in high-performance tokamaks. Further, the large reductions in the transport we observe when diamagnetic effects become moderately strong indicate that this non-MHD feature of the model also plays a vital role, and may in fact be central to the attainment of high-β edge plasmas in these machines.

[1] R. D. Sydora, Phys. Plasmas **2**, 1455 (1990).
[2] S. E. Parker *et al.*, Phys. Rev. Lett. **71**, 2042 (1993).
[3] R. E. Waltz *et al.*, Phys. Plasmas **2**, 2408 (1995).
[4] M. Kotschenreuther *et al.*, Phys. Plasmas **2**, 2381 (1995).
[5] A. M. Dimits *et al.*, Phys. Rev. Lett. **77**, 71 (1996).
[6] P. N. Guzdar *et al.*, Phys. Fluids B **3**, 3712 (1993).
[7] A. Zeiler *et al.*, Phys. Plasmas **3**, 2951 (1996).
[8] J. F. Drake *et al.*, Phys. Rev. Lett. **3**, 494 (1996).
[9] B. Scott, Plasma Phys. Controlled Fusion **39**, 471 (1997).
[10] P. L. Pritchett *et al.*, Phys. Fluids B **23**, 1368 (1980).